Geophysical Research Letters

RESEARCH LETTER
10.1029/2022GL098987

The Global Surface Area Variations of Lakes and Reservoirs as Seen From Satellite Remote Sensing

Matthew Bonnema[1], Cédric H. David[1], Renato Prata de Moraes Frasson[1], Catalina Oaida[1], and Sang-Ho Yun[2,3,4]

[1]Jet Propulsion Laboratory, California Institute of Technology, Pasadena, CA, USA, [2]Earth Observatory of Singapore, Nanyang Technological University, Singapore, Singapore, [3]Asian School of the Environment, Nanyang Technological University, Singapore, Singapore, [4]School of Electrical and Electronic Engineering, Nanyang Technological University, Singapore, Singapore

Key Points:

- Smaller water bodies show significantly more global sum total surface area variability than larger water bodies
- Reservoirs show more surface area variability than lakes of similar sizes
- Global intermittently inundated surface water body area is ~20% of its average, and small water bodies made up the most significant portion

Supporting Information:

Supporting Information may be found in the online version of this article.

Correspondence to:

M. Bonnema,
matthew.g.bonnema@jpl.nasa.gov

Citation:

Bonnema, M., David, C. H., Frasson, R. P. d. M., Oaida, C., & Yun, S.-H. (2022). The global surface area variations of lakes and reservoirs as seen from satellite remote sensing. *Geophysical Research Letters*, *49*, e2022GL098987. https://doi.org/10.1029/2022GL098987

Received 11 APR 2022
Accepted 6 JUL 2022

Abstract Natural lakes and artificial reservoirs are important components of the Earth system and essential for freshwater, food, and energy. Relatively little is known about the variations of lake and reservoir surface area globally. For the first time, this study presents the global variation of lake and reservoir surface areas for all water bodies larger than 1 km^2. Using radar remote sensing, we found that global aggregate area variations were only 2% of total surface area over a 3 year period. When considering the total surface area of shoreline regions that transition between land and water, these variations equaled 20% of total lake and reservoir surface area, largely driven by variations of smaller water bodies. Additionally, surface areas of reservoirs tends to be more variable than the surface area of lakes of similar size. The large surface area variations evidenced here, could have a previously underappreciated impact on the Earth System.

Plain Language Summary Natural lakes and artificial reservoirs are important parts of the Earth system and provide many benefits for humanity. Despite this importance, there are key things about lakes and reservoirs that are unknown globally, including how and when surface areas vary. This study uses satellite-based radar observations to estimate surface area variations in a set of the world's largest lakes and reservoirs. We found that the total surface area variability was relatively small when aggregated globally, only accounting for 2% of mean global surface water area. However, the total shoreline area that transitioned between water and land as a result of lake and reservoir variability was much more substantial, around 20% of mean global surface area. The variability of smaller water bodies contributed more to these transitional areas than larger water bodies. We also found that artificial reservoirs tended to be more variable than similarly sized natural lakes. Ultimately, the large surface area variations evidenced here, particularly in small water bodies, could have a previously underappreciated impact on the Earth System.

1. Introduction

Natural lakes and artificial reservoirs, hereafter referred to together as Surface Water Bodies (SWBs), storing 87% of Earth's surface liquid freshwater (Gleick, 1993), are critical components of the Earth system. SWBs have important influences over the hydrologic cycle (Müller Schmied et al., 2014), the carbon cycle (Cole et al., 2007), sediment and nutrient transport (Downing et al., 2008; Harrison et al., 2012), weather patterns (Balsamo et al., 2016), and climate change (Tranvik et al., 2009; Williamson et al., 2009; Wohlfahrt et al., 2021). SWBs also foster unique and diverse ecosystems (Abell et al., 2008; Gleick, 2003), provide a wide range of ecosystem services, such as food and water provisions (Postel & Carpenter, 1997; Schallenberg et al., 2013). Humanity derives additional societal benefit from artificial reservoirs, specifically hydroelectricity generation, flood mitigation, and recreation (Moran et al., 2018; Sterner et al., 2020).

The surface area of SWBs is a critical property as the water body surface is the medium through which SWBs interact with a number of Earth system processes, and is intimately connected with methane emissions (Bastviken et al., 2011), heat fluxes (Fink et al., 2014), and evaporation (Friedrich et al., 2018). As SWB area expands and contracts, shoreline areas experience intermittent inundation. These intermittently inundated areas are critical for gas emissions and plant phenology (Bastviken et al., 2004; Tranvik et al., 2009), and their magnitude is currently unknown globally. Surface area changes are also direct indicators of SWB storage changes, mediated by SWB hypsometry, which can inform on hydrologic processes, water resource management, availability of

water supply, and for reservoirs specifically, releases and operational procedures (Bonnema & Hossain, 2017). SWBs, and the hydrologic cycle as a whole, are undergoing changes due to anthropogenic activities and climate change (Grill et al., 2019; Haddeland et al., 2014; Rodell et al., 2018; Zarfl et al., 2015). Additionally, Wohlfahrt et al. (2021) have demonstrated that the increase in SWB area caused by the construction of artificial reservoirs lead to increased carbon emissions and decreases in albedo, which together affect the Earth's radiative budget. Thus, understanding changes to lake and reservoir surface areas, and how these changes translate to intermittently inundated areas, is critical for understanding changes in the hydrologic cycle and Earth system.

Much is known globally of the static state of SWB surface areas. Messager et al. (2016) created a database containing essential information such as location, nominal surface area, and spatial extent of all the world's SWBs. A number of other data sets provide similar static information globally, specifically for reservoirs (ICOLD, 1998; Lehner et al., 2011). Such information is vital for studying SWBs on the global scale, but lacks critical insight on temporal variability. SWBs are dynamic, expanding and contracting with the seasonal cycle and on longer time scales in response to changes in infrastructure, water use, and to natural and anthropogenic changes to the water cycle. A deeper understanding of these seasonal and interannual changes globally are beyond the limits of the current state of knowledge.

On more localized scales, many remote sensing based techniques have been developed to monitor lake and reservoir dynamics, with some dating back nearly three decades (e.g., Birkett, 1994). In the time since these early applications, methods for utilizing data from many different sensors have been well established (Gao, 2015) and applied to a wide variety of lakes and regions (DeVries et al., 2017; Gao et al., 2012; Jones, 2015, 2019; Phan et al., 2012; Schwatke et al., 2019; X. Wang et al., 2013; Zhang et al., 2014). Despite this depth of research, there are still fundamental gaps in our understanding of SWB area dynamics at global scales. Long term trends in storage dynamics are equally unknown globally and it is unclear how SWB variability will change in response to future changes in the climate (Woolway et al., 2020). In fact, even the magnitude of seasonal lake and reservoir variations is poorly understood globally (Lettenmaier et al., 2015), with recent efforts utilizing water elevation observations to quantify water level variations only recently appearing in the literature (Cooley et al., 2021). These gaps in knowledge lead to uncertainties in characterizations of hydrological budgets (Müller Schmied et al., 2014), land surface modeling (Balsamo et al., 2016), and the responses and contributions of lakes to climate change (Williamson et al., 2009).

Recent remote sensing based efforts to fill our gaps in knowledge of global SWB dynamics (Biswas et al., 2020; Busker et al., 2019; Zhao & Gao, 2018) have been enabled by the advent of accessible cloud computing platforms such as Google Earth Engine (GEE; Gorelick et al., 2017), which offers powerful computing of the big data needed to study SWBs in a globally complete way and studies such as Pekel et al. (2016) have leveraged these platforms to provide global scale information about surface water as a whole. However, cloud computing-based efforts have not yet focused on surface area variations of SWBs globally. Furthermore, many larger scale SWB studies rely on optical imagery (Biswas et al., 2020; Busker et al., 2019; Chen et al., 2021; Gao et al., 2012; Meyer et al., 2020; Yao et al., 2019; Zhang et al., 2014), which is regularly blocked by clouds, hindering its ability to capture the complete seasonal cycle of SWB dynamics in much of the world, where persistent seasonal cloudiness is common. Because Synthetic Aperture Radar (SAR) can penetrate clouds, water detection methods that make use of SAR data are less susceptible to cloud cover, hence the use of platforms such as Sentinel-1 to automatically detect and map floods (Yang et al., 2021). Despite the existence of automated unsupervised SAR-based water detection methods (e.g., Liang & Liu, 2020), such methods are yet to be used to quantify SWB surface area dynamics globally.

The overarching goal of this study is to answer the following fundamental earth science questions: *What are the seasonal surface area variations of SWBs globally, are there fundamental differences between the surface area variability of natural lakes and artificial reservoirs, and what is the total surface area of intermittently inundated areas?* This paper leverages the frequent, high resolution C-band SAR observations from the Copernicus Sentinel-1 mission to reveal the global variability of lake and reservoir water surface areas for the first time. This study aims to derive fundamental knowledge of seasonal lake dynamics, a valuable data set of large lake surface area variations, and a simple, cloud computing-ready methodology.

2. Methods

The approach developed here to quantify lake surface area and surface area variations globally from Sentinel-1 SAR data requires four key ingredients: (a) a static database of SWBs to locate and identify regions of interest (solid black line in Figure 1a); (b) a static water probability map (gray scale in Figure 1a) to identify persistent water and persistent land regions (blue and brown regions in Figure 1b, respectively); (c) an efficient water classification algorithm that is applicable to any time and location on earth, and (d) a computing platform powerful enough to run the classification algorithm globally in a reasonable amount of time. The HydroLAKES database (Messager et al., 2016) was used here to identify SWBs, differentiate between lakes and reservoirs, and provide SWB locations and boundaries. For the cloud computing platform, GEE was used because of its raster processing computational power and its native hosting of the Sentinel-1 data sets, eliminating the need for download or storage of large data locally. In general, the classification approach developed here identifies water based on Sentinel-1 SAR backscatter, which is generally much lower from water than land (Figure 1).

The water surface area classification algorithm operates on individual SWB. For any given SWB, the static water body boundary shapefile is selected from HydroLAKES and buffer around the boundary is created, forming the region of interest (ROI) for the classification. Buffer size is scaled according to nominal water body area using the same approach as Biswas et al. (2020). Scenes that overlap the ROI are identified from the Sentinel-1 SAR Ground Range Detected product (available in GEE), which contains 10 m pixel spacing, calibrated, and ortho-corrected gridded backscatter images (Geudtner et al., 2014). First, a speckle filter is applied to each backscatter image (Filipponi, 2019) and then they are averaged monthly, to provide a monthly mosaic of the entire lake and surrounding area.

Our new water classification method uses a backscatter (σ_0) thresholding approach, where pixels with σ_0 lower than a certain water detection threshold (σ_{0WD}) are classified as water. This approach relies on the principle that C-band SAR σ_0 at inclination angles between 30 and 42° (Sentinel-1 SAR instrument inclination angle range) is significantly lower over water than over land. However, the appropriate threshold is dependent on both the condition of the water (waves and aquatic vegetation) and the condition of the surrounding land (vegetation, soil moisture, and slope). To identify an appropriate σ_0 threshold automatically for any individual SWB and for any given time, a static water occurrence map derived from 40 years of visible Landsat data, from the Global Surface Water Dataset (GSW; Pekel et al., 2016) is used. Here, these water occurrence probabilities are used to identify regions that are very likely to be water (water probability equal to the greatest water probability within ROI) and regions very unlikely to be water (water probability equal to 0% within the ROI).

The pixels in each monthly backscatter mosaic are then sampled from both the likely water regions and the likely land regions, within the ROI (Figures 1a and 1b) and the backscatter mean (M) and standard deviation (S) of both water and land samples are calculated for each monthly mosaic. The classification threshold (σ_{0WD}) given by Equation 1, where S_{Water} and S_{Land} represent the standard deviations of the water and land pixel backscatter respectively, M_{Water} and M_{Land} stand for the means of the water and land pixel backscatter, and x is a multiplicative factor found by equating the center and the right-hand side terms of Equation 1 (Figure 1d). Note that this threshold selection process is similar to that applied to optical observations in Li and Sheng (2012) and Sheng et al. (2016). Then, all pixels of the monthly mosaic within the ROI are classified as water if their σ_0 is less than the threshold, and not water if σ_0 is greater than the threshold (Equation 2). Because of variable land conditions (e.g., vegetation and soil moisture) and variable water conditions (e.g., waves, aquatic vegetation, and ice), thresholds are uniquely defined for each lake and for each monthly time step. This results in a classification scheme that is robust to both geographical and temporal variations in land-water contrast.

$$\sigma_{0WD}(t) = M_{Water}(t) + xS_{Water}(t) = M_{Land}(t) - xS_{Land}(t) \tag{1}$$

$$\text{class}(x, y, t) = \begin{cases} \text{water} & \text{if } \sigma_0(x, y, t) \leq \sigma_{0WD}(t) \\ \text{land} & \text{if } \sigma_0(x, y, t) > \sigma_{0WD}(t) \end{cases} \tag{2}$$

Next, the total surface area of water pixels is calculated by multiplying the number of classified water pixels by the grid cell size (100 m^2). This is repeated for each monthly mosaic, producing a monthly time series of SWB surface area. Several factors can cause a monthly area estimate to fail, including incomplete monthly SAR

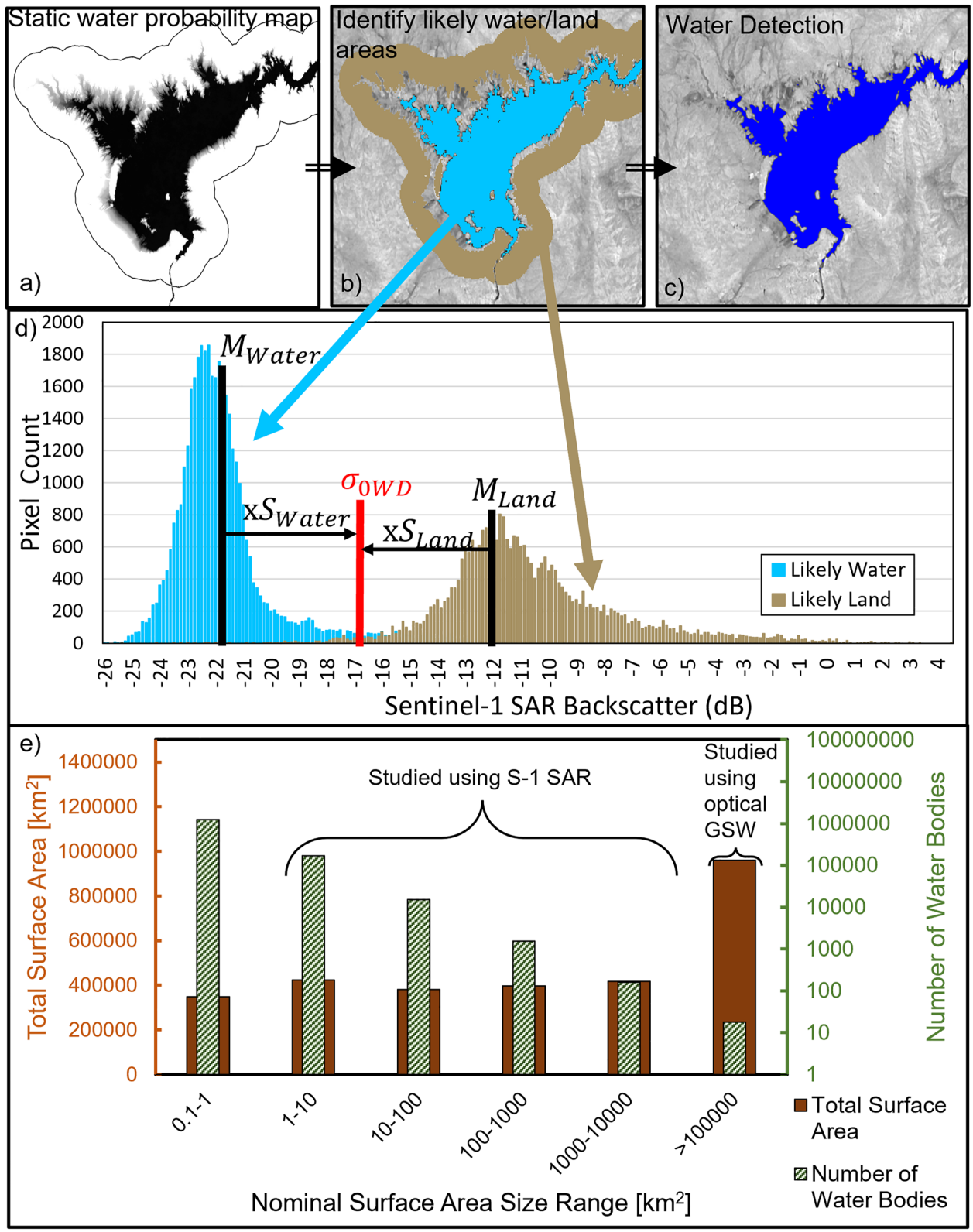

Figure 1.

coverage of the ROI. These missing monthly surface area estimates are represented by no-data flags in the data set and are recovered in the analysis by linearly interpolating neighboring monthly surface areas. If more than three consecutive months (one season) of surface areas are interpolated, the time series is removed from the final analysis. Classification errors were also estimated, and a detailed description of this process can be found in Text S1 in Supporting Information S1. Monthly surface area estimates with high classification errors (greater than 20% of nominal water body area) were also removed and interpolated from neighboring values.

The HydroLAKES database identifies over 1.4 million SWBs with surface areas greater than 0.1 km^2, and was used here because of its carefully delineated shoreline boundaries (Messager et al., 2016), which simplify much of the classification approach. This study focuses on global SWBs with surface areas greater than 1 km^2, which, according to the nominal areas listed in the HydroLAKES database (Messager et al., 2016), account for 88% of total global SWB surface area (Figure 1e). This lower limit of 1 km^2 was selected due to technical limitations of applying the algorithm to the 1.2 million SWBs smaller than 1 km^2 (see Text S2 in Supporting Information S1). A feature of HydroLAKES is that water bodies are defined as natural lakes by default and only defined as artificial reservoirs if explicitly identified as a reservoir, and thus all unidentified smaller reservoirs are labeled as lakes in the database. To correct for this, the HydroLAKES database was spatially joined with GeoDAR, a global reservoir data set (J. Wang et al., 2022). This process changes the classification of 1,968 water bodies from lakes to reservoirs, mostly ranging in size from 1 to 10 km^2.

There is also an upper limit on the size of water bodies that can be classified using the SAR classification method presented here. Extremely large water bodies regularly extend across many Sentinel-1 swaths, leading to larger variability in SAR backscatter (σ, in dB) contrast between land and water, invalidating our assumption of a uniform classification threshold across the water body. For this reason, the dynamics of the 18 water bodies with surface areas greater than 10,000 km^2 were not estimated using the method described above. Instead, we calculated areas of these 18 SWBs using the European Joint Research Center (JRC) GSW maps produced according to the methodology published in Pekel et al. (2016). The processing of these Landsat-derived monthly water occurrence maps mirrored the processing of the SAR-derived inundation maps, where the lake surface area was estimated by summing the area of water pixels contained in each ROI. Inundation maps with more than 2% no-data pixels (due to cloud cover or other data quality issues), were removed and surface area values were interpolated from neighboring observations.

This same approach was also used in a comparison between the SWB surface areas derived here with SAR and SWB surface areas derived from the JRC GSW data set for all SWBs between 1 and 10,000 km^2. This comparison, consisting of over 400,000 coincidental SWB surface area observations, shows strong agreement between the two data sets derived from two different sensor technologies. For a more detailed description of this comparison, see Text S2 in Supporting Information S1.

3. Results and Discussion

The map in Figure 2a shows the location and relative size of all natural lakes and artificial reservoirs studied here, 156,045 SWBs in total. Figure 2b zooms in to show the western US. Here, lake and reservoir surface areas are represented by circle size, where the minimum area observed in the 3-year time period (2017–2019) is represented by the lighter colored inner circles, and the maximum observed area is represented by the outer, darker circles. In other words, water bodies with larger portions of the darker circles visible showed a larger range (i.e., difference between maximum and minimum area), an indication of higher variability in surface area. What is clear from this figure is that even across this relatively small geographical area, the amplitudes of surface area variation were highly variable, with some SWBs showing almost no variation, while others varied significantly. Zooming in further, Figures 2c and 2d show surface area time series of an artificial reservoir in Brazil (Tres Marias Reservoir) and a natural lake in the Philippines (Laguna Lake). These individual time series highlight the granularity of our results, that behind every circle in Figure 2a, there is a 3-year long monthly surface area time

Figure 1. Example images of Lake Mead (Arizona-Nevada, USA) showing the water body classification methodology, where the static water mask in greyscale (a) is used to identify regions that are likely water and regions that are likely land within the area surrounding the lake boundary (Pekel et al., 2016). The Synthetic Aperture Radar (SAR) backscatter within likely land and likely water regions are sampled to determine the appropriate classification threshold (b), and this threshold is applied to the entire SAR backscatter mosaic within the region of interest to identify inundated pixels (c). (d) A histogram of backscatter pixel values for Lake Mead example image, for areas likely to be water and those likely to be land, as well as the selected classification threshold. (e) Also shown is a dual histogram of SWB count and total surface area of different orders of magnitude, both taken from the HydroLAKES Database (Messager et al., 2016).

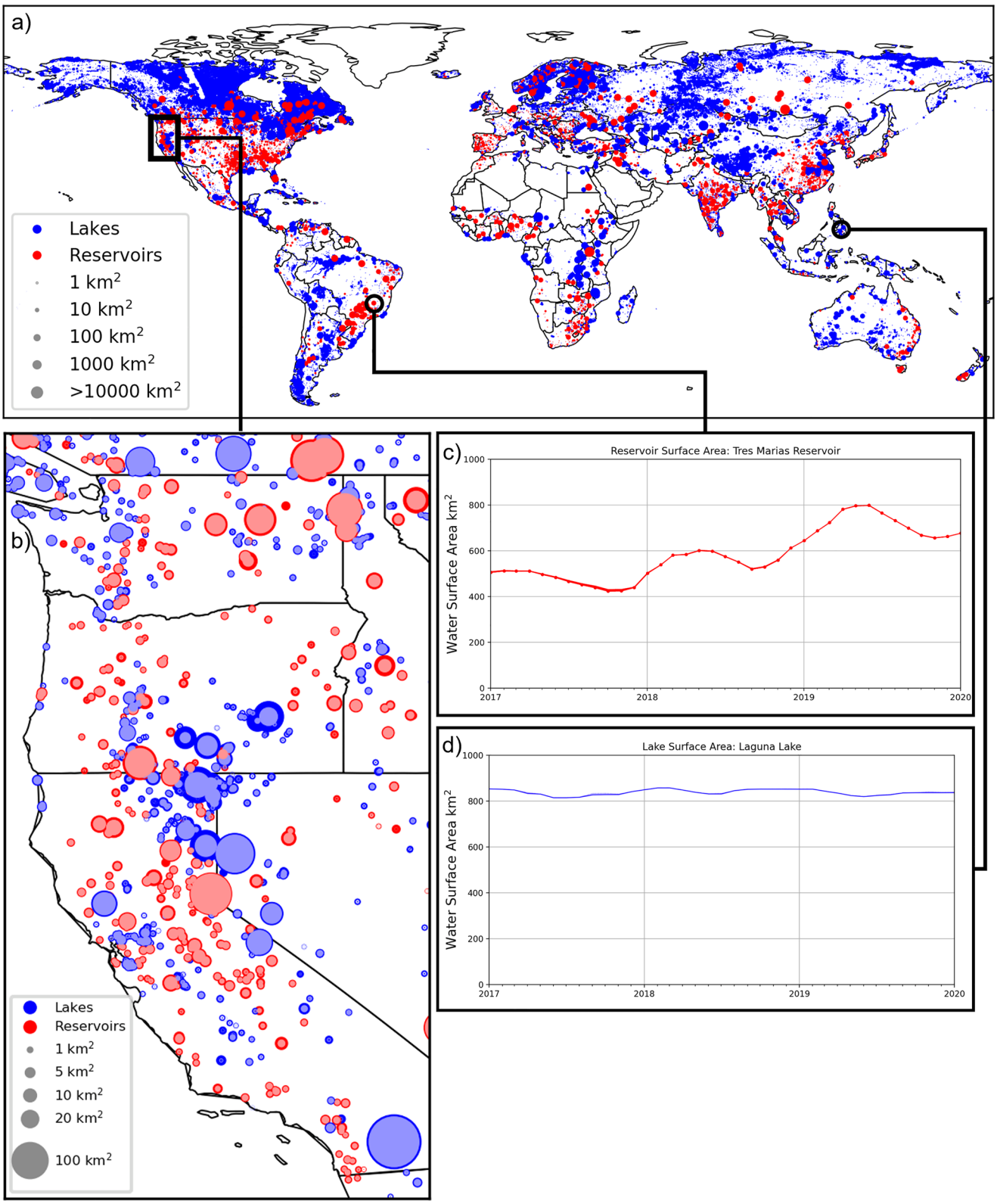

Figure 2. (a) Global map showing locations and relative size of 150,000 lakes and reservoirs studied here. (b) Excerpt of the western US, showing lake and reservoir surface area minimum (lightly colored circled) and maximum (darkly colored circles) observed in study period. Larger differences in size between the light and dark circles for any given Surface Water Body indicate higher variability. (c) Example of individual reservoir time series from Tres Marias Reservoir in Brazil showing seasonality. (d) Example of individual lake time series from Laguna Lake in the Philippines showing seasonality.

series. In both example time series, we see seasonal variations, with the Tres Marias Reservoir showing much more variability than Laguna Lake. While there are a number of reasons for water bodies to have different levels of variability (e.g., hypsometry, geography, climate, and anthropogenic activities), this study explores two key factors that appear to influence this variability, water body size and whether a water body is natural or artificial.

However, before we investigate patterns in surface area variability, we first seek to understand how the surface area of the world's SWBs are varying on the whole. To do this, the individual lake and reservoir surface area time series were summed, providing a global total surface area time series for all SWBs, and both lakes and reservoirs separately, shown in Figure 3a. Here, the 18 water bodies larger than 10,000 km^2 are shown separately, because of the different method in which they were estimated, as well as their considerably lower variability, which is explored in subsequent paragraphs. The most apparent feature of these time series is that the global spatial sum of temporally averaged-surface area (hereafter referred to as global-sum) for lakes in this study was 7.5 times that of the set of study reservoirs, with global-sum surface area of 1.82 million km^2 and global-sum reservoir area of 268,000 km^2. Also apparent in the time series are seasonal signals in both lakes and reservoirs, which then manifest in the total SWB surface area time series. However, this variability appears small relative to total surface area. The relatively small magnitude of this global variability is not surprising, as SWBs from around the world follow different seasonal patterns, usually tied to both natural and anthropogenic variations in surface water availability. These differently timed signals are expected to cancel out to some extent when aggregated to the global scale. Still, this result is significant simply because this is the most complete estimate global surface area variability to date.

To more closely investigate the monthly variability of these time series, aggregate surface area anomalies were calculated by subtracting the mean total surface area from each time series (excluding water bodies larger than 10,000 km^2), the results of which are shown in Figure 3b. Despite the competing seasonal signals from over 150,000 water bodies, the overall temporal variations of both lakes and reservoirs are visible, with clear seasonal variability, typically ranging from $\pm$10,000 km^2. The total area anomalies of natural lakes and artificial reservoirs are similar in magnitude, which is surprising given that the total surface area of lakes (smaller than 10,000 km^2) is nearly four times that of reservoirs in this study. This indicates that reservoirs vary more than lakes, as suggested by the individual SWB scale analysis. Another way of interpreting these anomalies is that the difference between the natural lake surface area anomaly and the total SWB anomaly is the amount of total surface area variability created through anthropogenic dam development. There appears to be an approximately 4-month lag between artificial reservoir and natural lake surface area anomalies. Such timing differences are expected on smaller scales because reservoirs releases and withdrawals (which in turn affects lake storage and surface area) are dictated by human needs and often do not align with the natural hydrologic cycle, unlike lakes. However, such a lag between lakes and reservoirs at the global scale was not guaranteed.

While the magnitude of total surface area variations is similar for natural lakes and artificial reservoirs, if these anomalies are presented as a percentage of average surface area (Figure 3c), the amplitude of global aggregates reservoir variations (5.2%) becomes significantly greater than that of lakes (1.9%). This is another indication that reservoir surface area may be more variable than lakes and is in agreement with Cooley et al. (2021), which found that global average reservoir water level variations were approximately 4 times greater than those of natural lakes. Also apparent in this figure is a significant difference between the area anomalies of all SWBs and of natural lakes, indicating again that reservoir area variations are fairly significant on the global scale, despite making up only a small portion of total surface area. Note that there is a big limitation of this global aggregate analysis that was alluded to earlier, that different water bodies follow different seasonal signals, which cancel out when aggregating on the global scale, dampening the variability of individual water bodies. However, this analysis does provide a useful lower bound to surface area variability, that even if the entire earth surface is considered as a single unit, SWB surface area still shows seasonal variability, albeit relatively small variability.

Next, we examine the opposite end of the spectrum, by investigating the variability on individual water body scales. By only considering the amplitude of variability, SWB area variability can be globally analyzed without interference from differently timed seasonal signals. This allows for the identification of patterns in variability among SWBs. Figure 4a shows one such pattern by grouping SWBs by their nominal surface area (taken from the HydroLAKES Database) and then plotting the quartiles of variability relative to average surface area (from estimated surface area time series). This plot shows a very clear trend, that smaller SWBs are more variable on average, and have the potential for extreme surface area variations. The increased variability of smaller water

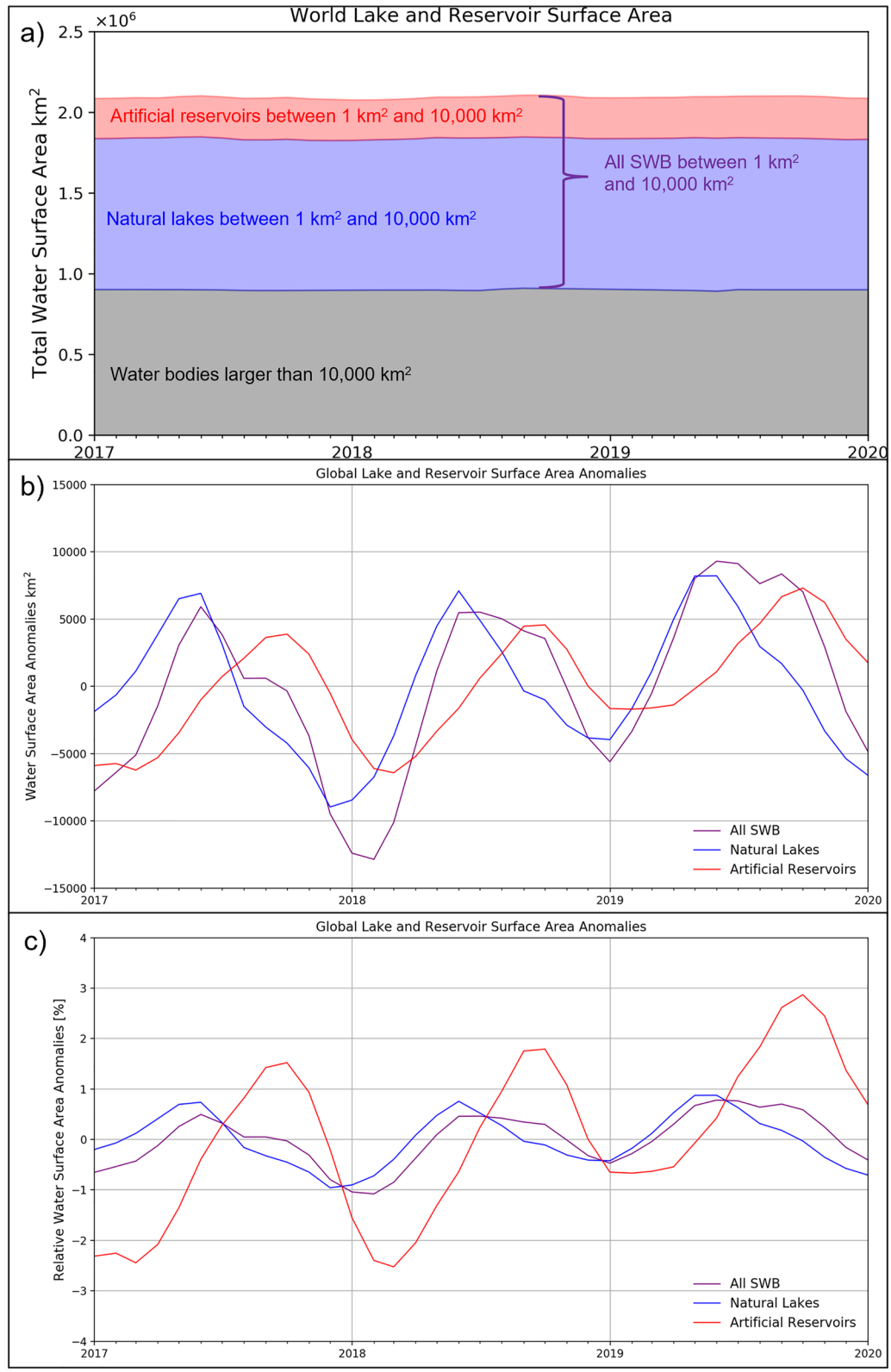

Figure 3. (a) Global total surface area time series of lakes and reservoirs, computed by summing the surface area time series of individual lakes and reservoirs. (b) Global aggregate surface area anomalies, computed by subtracting mean total storage from total storage time series. (c) Global aggregate surface area anomalies as a percentage of total mean storage.

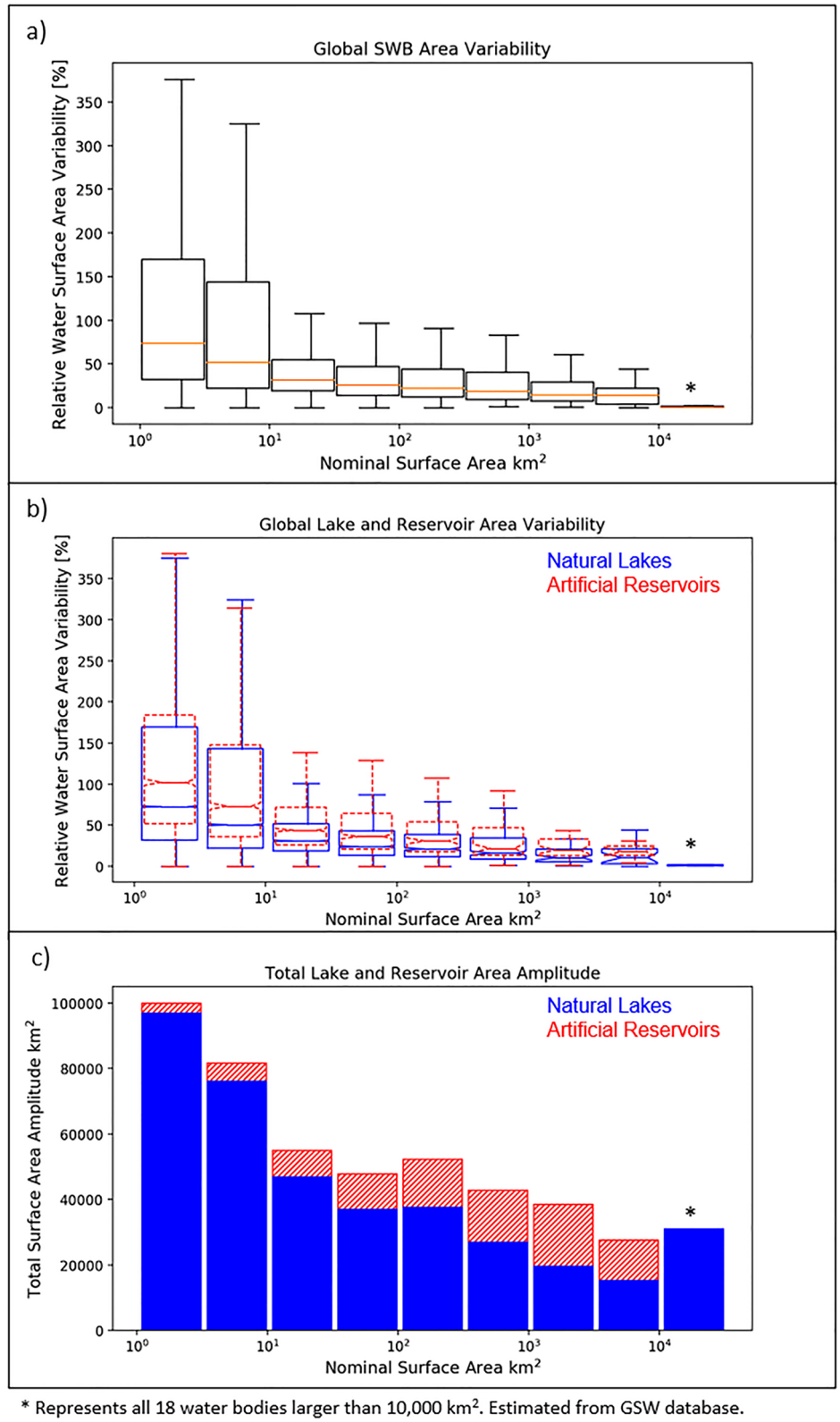

Figure 4. (a) Relative water surface area variability of individual Surface Water Bodies (SWBs), grouped by size classes, delineated by half orders of magnitude. Panel (b) same plot as panel (a), but each size class is separated into natural lakes and artificial reservoirs. (c) Sum total of the surface area amplitude of individual SWBs in each size class.

bodies is quite substantial as well, with the smallest size class (from 1 to $10^{1/2}$ km^2) having a median surface area variability of 74%. This trend appears to hold across all four orders of magnitude of SWB area studied with SAR, as well as the largest set of water bodies studied with the GSW data set. In fact, these 18 water bodies larger than 10,000 km^2 showed extremely small relative variability.

Figure 4b shows a similar plot, but with lakes and reservoir separated within each surface area class. This plot shows that within this size trend, artificial reservoirs are consistently more variable than natural lakes, especially when comparing the medians of each area class. In fact, for many area classes, median reservoir variability is similar to the third quartile lake variability (e.g., between 10^3 and 10^4 km^2). The larger variations of reservoirs agree with the significant global reservoir surface area aggregates shown in Figure 3. However, this feature is not universal and there were many lakes with significant area variations, as evidenced by the larger variability ranges in some of the area classes (e.g., 1–10 and 10^3–10^4 km^2). That is to say, the surface area of some natural lakes, especially small natural lakes, can vary significantly. However, it is not clear from Figure 4b alone whether the high relative variations of small SWBs translate to meaningful total seasonally inundated area.

While surface area variations of global SWBs are largely out of phase and cancel out when summed (as evidenced by Figure 2), the amplitudes of surface area variation of individual SWBs can be summed to quantify the total seasonally inundated area. Figure 4c shows the global total seasonally inundated area for each SWB area size class, illustrating that the higher relative area variability of smaller SWBs (shown in Figure 4b) manifests in higher total seasonally inundated areas. In total, this variable area adds up to 476,000 km^2, or approximately 20% of total average SWB surface area (greater than 1 km^2). It is clear that the variations of small water bodies (smaller than 10 km^2) make up a significant amount of this overall seasonally inundated area (the sum of all columns in Figure 4c), accounting for 37% of the total seasonally inundated area. When comparing the total seasonal area of natural lakes and reservoirs, it appears that reservoir total seasonal area declines for smaller size classes. However, this may be an artifact of a limitation of the HydroLAKES Database, where smaller reservoirs, especially below 10 km^2, are under-identified, and are instead labeled as natural lakes. Even though a correction to water body classification was applied using GeoDAR to mitigate this issue, there may be additional small artificial water bodies not captured by this process. This means that while the total seasonal area would remain the same, some of the area attributed to lakes in the smaller size classes, actually belongs to reservoirs. Future work should make use of newer reservoir data sets such as GeoDAR, to properly identify small artificial reservoirs.

4. Conclusion

Using SAR data from Sentinel-1 at a global scale in combination with harnessing cloud computing capabilities, this study provides for the first time, a world view of large lake and reservoir surface area variations and directly addresses a fundamental gap in knowledge, the intra-annual magnitude of lake and reservoir variations globally (Lettenmaier et al., 2015). Our 3 year analysis of over 150,000 lakes and reservoirs suggests that the seasonally inundated surface area of SWBs is significant, adding up to approximately 20% of the total lake and reservoir surface area. We also found a clear relationship between a water body size and surface area variability, with smaller water bodies, especially those with areas less than 10 km^2, showing higher variability on average, as well as the potential for extreme surface area variations. In addition, our results showed that while these high variations occur in small water bodies, these variations contribute to a substantial portion of the global seasonally inundated area. These findings suggest that even smaller water bodies (e.g., the 1.2 million water bodies between 0.1 and 1 km^2) could be more variable individually, and could have more significant contributions to seasonally inundated areas. This highlights the importance of both further research into novel cloud computing based remote sensing methods, targeted at smaller water bodies, as well as future remote sensing missions such as the Surface Water and Ocean Topography Mission, which is expected to observe all lakes larger than 0.0625 km^2 (Biancamaria et al., 2016).

Our findings also have implications for better understanding the Earth system. These lake and reservoir surface area variations are indicative of changes in surface water storage, which is a key component of the hydrologic cycle as well as an essential source of freshwater, food, and energy. More directly, the implication of these findings to the modeling of various Earth systems, such as land surface models, carbon cycle models, or methane emission models, is that lake and reservoir surface areas can often be very dynamic and need to be taken into account, as the results here show that 20% of the total global area of water bodies larger than 1 km^2 changes

between land and water seasonally. This is especially significant in the context of carbon and methane emissions, which both depend on water body surface area, and have been shown to have large contributions from smaller water bodies (Holgerson & Raymond, 2016). Ultimately, understanding lake and reservoir surface area is important to understanding the earth system as a whole, and this study provides a first of its kind window into the area variations of large lakes and reservoirs, as well as a simple, globally applicable method for deriving area variations of any lake or reservoir in the world.

Data Availability Statement

The authors would like to acknowledge Bruno Collischonn of the Brazilian National Water and Sanitation Agency (ANA) for his help locating the data (https://www.ana.gov.br/sar0/MedicaoSin) used for the validation of the Tres Marias Reservoir surface area measurements shown in Figure S2 in Supporting Information S1. Note that this site is only available in Portuguese, but any user can locate the elevation data by selecting "TRES MARIAS" as the "Reservatório," export with the "Exportar" button, and then reading the "Cota" (elevation) and "Data da Medição" (acquisition date) columns. Copernicus Sentinel-1 data (2017–2019), was obtained from Google Earth Engine (GEE; https://developers.google.com/earth-engine/datasets/catalog/COPERNICUS_S1_GRD). Pekel et al. (2016) data was obtained from GEE (https://developers.google.com/earth-engine/datasets/catalog/JRC_GSW1_3_MonthlyHistory). HydroLAKES data set was obtained from https://www.hydrosheds.org/page/hydrolakes. The software developed for this study is available at https://doi.org/10.5281/zenodo.6450466. The output data is available at https://doi.org/10.5281/zenodo.6345234.

Acknowledgments
This work was supported by the Jet Propulsion Laboratory, California Institute of Technology, under a contract with the U.S. National Aeronautics and Space Administration (NASA), including projects funded under NASA's Terrestrial Hydrology Program (NNH17ZDA001N-THP) and Surface Water and Ocean Topography Science Team (NNH15ZDA001N-SWOT); as well as JPL's Strategic Research and Technology Development. Government sponsorship is acknowledged.

References

Abell, R., Thieme, M. L., Revenga, C., Bryer, M., Kottelat, M., Bogutskaya, N., et al. (2008). Freshwater ecoregions of the world: A new map of biogeographic units for freshwater biodiversity conservation. *BioScience*, *58*(5), 403–414. https://doi.org/10.1641/B580507

Balsamo, G., Salgado, R., Dutra, E., Boussetta, S., Stockdale, T., & Potes, M. (2016). On the contribution of lakes in predicting near-surface temperature in a global weather forecasting model. *Tellus A: Dynamic Meteorology and Oceanography*, *68*(s1), 15829. https://doi.org/10.3402/tellusa.v64i0.15829

Bastviken, D., Cole, J., Pace, M., & Tranvik, L. (2004). Methane emissions from lakes: Dependence of lake characteristics, two regional assessments, and a global estimate. *Global Biogeochemical Cycles*, *18*(4), GB4009. https://doi.org/10.1029/2004GB002238

Bastviken, D., Tranvik, L. J., Downing, J. A., Crill, P. M., & Enrich-Prast, A. (2011). Freshwater methane emissions offset the continental carbon sink. *Science*, *331*(6013), 50. https://doi.org/10.1126/science.1196808

Biancamaria, S., Lettenmaier, D. P., & Pavelsky, T. M. (2016). The SWOT mission and its capabilities for land hydrology. In A. Cazenave, N. Champollion, J. Benveniste, & J. Chen (Eds.), *Remote sensing and water resources* (pp. 117–147). Springer International Publishing. https://doi.org/10.1007/978-3-319-32449-4_6

Birkett, C. M. (1994). Radar altimetry: A new concept in monitoring lake level changes. *Eos, Transactions American Geophysical Union*, *75*(24), 273–275. https://doi.org/10.1029/94EO00944

Biswas, N. K., Hossain, F., Bonnema, M., Aminul Haque, A. M., Biswas, R. K., Bhuyan, A., & Hossain, A. (2020). A computationally efficient flash flood early warning system for a mountainous and transboundary river basin in Bangladesh. *Journal of Hydroinformatics*, *22*(6), 1672–1692. https://doi.org/10.2166/hydro.2020.202

Bonnema, M., & Hossain, F. (2017). Inferring reservoir operating patterns across the Mekong Basin using only space observations. *Water Resources Research*, *53*(5), 3791–3810. https://doi.org/10.1002/2016WR019978

Busker, T., de Roo, A., Gelati, E., Schwatke, C., Adamovic, M., Bisselink, B., et al. (2019). A global lake and reservoir volume analysis using a surface water dataset and satellite altimetry. *Hydrology and Earth System Sciences*, *23*(2), 669–690. https://doi.org/10.5194/hess-23-669-2019

Chen, T., Song, C., Ke, L., Wang, J., Liu, K., & Wu, Q. (2021). Estimating seasonal water budgets in global lakes by using multi-source remote sensing measurements. *Journal of Hydrology*, *593*, 125781. https://doi.org/10.1016/j.jhydrol.2020.125781

Cole, J. J., Prairie, Y. T., Caraco, N. F., McDowell, W. H., Tranvik, L. J., Striegl, R. G., et al. (2007). Plumbing the global carbon cycle: Integrating inland waters into the terrestrial carbon budget. *Ecosystems*, *10*(1), 172–185. https://doi.org/10.1007/s10021-006-9013-8

Cooley, S. W., Ryan, J. C., & Smith, L. C. (2021). Human alteration of global surface water storage variability. *Nature*, *591*(7848), 78–81. https://doi.org/10.1038/s41586-021-03262-3

DeVries, B., Huang, C., Lang, M. W., Jones, J. W., Huang, W., Creed, I. F., & Carroll, M. L. (2017). Automated quantification of surface water inundation in wetlands using optical satellite imagery. *Remote Sensing*, *9*(8), 807. https://doi.org/10.3390/rs9080807

Downing, J. A., Cole, J. J., Middelburg, J. J., Striegl, R. G., Duarte, C. M., Kortelainen, P., et al. (2008). Sediment organic carbon burial in agriculturally eutrophic impoundments over the last century. *Global Biogeochemical Cycles*, *22*(1), GB1018. https://doi.org/10.1029/2006GB002854

Filipponi, F. (2019). Sentinel-1 GRD preprocessing workflow. *Proceedings*, *18*(1), 11. https://doi.org/10.3390/ECRS-3-06201

Fink, G., Schmid, M., Wahl, B., Wolf, T., & Wüest, A. (2014). Heat flux modifications related to climate-induced warming of large European lakes. *Water Resources Research*, *50*(3), 2072–2085. https://doi.org/10.1002/2013WR014448

Friedrich, K., Grossman, R. L., Huntington, J., Blanken, P. D., Lenters, J., Holman, K. D., et al. (2018). Reservoir evaporation in the Western United States: Current science, challenges, and future needs. *Bulletin of the American Meteorological Society*, *99*(1), 167–187. https://doi.org/10.1175/BAMS-D-15-00224.1

Gao, H. (2015). Satellite remote sensing of large lakes and reservoirs: From elevation and area to storage. *WIREs Water*, *2*(2), 147–157. https://doi.org/10.1002/wat2.1065

Gao, H., Birkett, C., & Lettenmaier, D. P. (2012). Global monitoring of large reservoir storage from satellite remote sensing. *Water Resources Research*, *48*(9), 2012WR012063. https://doi.org/10.1029/2012WR012063

Geudtner, D., Torres, R., Snoeij, P., Davidson, M., & Rommen, B. (2014). Sentinel-1 system capabilities and applications. In *2014 IEEE Geoscience and Remote Sensing Symposium* (pp. 1457–1460). https://doi.org/10.1109/IGARSS.2014.6946711

Gleick, P. H. (1993). Water and conflict: Fresh water resources and international security. *International Security*, *18*(1), 79–112. https://doi.org/10.2307/2539033

Gleick, P. H. (2003). Global freshwater resources: Soft-path solutions for the 21st century. *Science*, *302*(5650), 1524–1528. https://doi.org/10.1126/science.1089967

Gorelick, N., Hancher, M., Dixon, M., Ilyushchenko, S., Thau, D., & Moore, R. (2017). Google Earth Engine: Planetary-scale geospatial analysis for everyone. *Remote Sensing of Environment*, *202*, 18–27. https://doi.org/10.1016/j.rse.2017.06.031

Grill, G., Lehner, B., Thieme, M., Geenen, B., Tickner, D., Antonelli, F., et al. (2019). Mapping the world's free-flowing rivers. *Nature*, *569*(7755), 215–221. https://doi.org/10.1038/s41586-019-1111-9

Haddeland, I., Heinke, J., Biemans, H., Eisner, S., Flörke, M., Hanasaki, N., et al. (2014). Global water resources affected by human interventions and climate change. *Proceedings of the National Academy of Sciences*, *111*(9), 3251–3256. https://doi.org/10.1073/pnas.1222475110

Harrison, J. A., Frings, P. J., Beusen, A. H. W., Conley, D. J., & McCrackin, M. L. (2012). Global importance, patterns, and controls of dissolved silica retention in lakes and reservoirs. *Global Biogeochemical Cycles*, *26*(2), GB2037. https://doi.org/10.1029/2011GB004228

Holgerson, M. A., & Raymond, P. A. (2016). Large contribution to inland water CO_2 and CH_4 emissions from very small ponds. *Nature Geoscience*, *9*(3), 222–226. https://doi.org/10.1038/ngeo2654

ICOLD. (1998). *World register of dams*. International Commission on Large Dams Paris.

Jones, J. W. (2015). Efficient wetland surface water detection and monitoring via Landsat: Comparison with in situ data from the everglades depth estimation network. *Remote Sensing*, *7*(9), 12503–12538. https://doi.org/10.3390/rs70912503

Jones, J. W. (2019). Improved automated detection of subpixel-scale inundation—Revised dynamic surface water extent (DSWE) partial surface water tests. *Remote Sensing*, *11*(4), 374. https://doi.org/10.3390/rs11040374

Lehner, B., Liermann, C. R., Revenga, C., Vörösmarty, C., Fekete, B., Crouzet, P., et al. (2011). High-resolution mapping of the world's reservoirs and dams for sustainable river-flow management. *Frontiers in Ecology and the Environment*, *9*(9), 494–502. https://doi.org/10.1890/100125

Lettenmaier, D. P., Alsdorf, D., Dozier, J., Huffman, G. J., Pan, M., & Wood, E. F. (2015). Inroads of remote sensing into hydrologic science during the WRR era. *Water Resources Research*, *51*(9), 7309–7342. https://doi.org/10.1002/2015WR017616

Li, J., & Sheng, Y. (2012). An automated scheme for glacial lake dynamics mapping using Landsat imagery and digital elevation models: A case study in the Himalayas. *International Journal of Remote Sensing*, *33*(16), 5194–5213. https://doi.org/10.1080/01431161.2012.657370

Liang, J., & Liu, D. (2020). A local thresholding approach to flood water delineation using Sentinel-1 SAR imagery. *ISPRS Journal of Photogrammetry and Remote Sensing*, *159*, 53–62. https://doi.org/10.1016/j.isprsjprs.2019.10.017

Messager, M. L., Lehner, B., Grill, G., Nedeva, I., & Schmitt, O. (2016). Estimating the volume and age of water stored in global lakes using a geo-statistical approach. *Nature Communications*, *7*(1), 13603. https://doi.org/10.1038/ncomms13603

Meyer, M. F., Labou, S. G., Cramer, A. N., Brousil, M. R., & Luff, B. T. (2020). The global lake area, climate, and population dataset. *Scientific Data*, *7*(1), 174. https://doi.org/10.1038/s41597-020-0517-4

Moran, E. F., Lopez, M. C., Moore, N., Müller, N., & Hyndman, D. W. (2018). Sustainable hydropower in the 21st century. *Proceedings of the National Academy of Sciences*, *115*(47), 11891–11898. https://doi.org/10.1073/pnas.1809426115

Müller Schmied, H., Eisner, S., Franz, D., Wattenbach, M., Portmann, F. T., Flörke, M., & Döll, P. (2014). Sensitivity of simulated global-scale freshwater fluxes and storages to input data, hydrological model structure, human water use and calibration. *Hydrology and Earth System Sciences*, *18*(9), 3511–3538. https://doi.org/10.5194/hess-18-3511-2014

Pekel, J.-F., Cottam, A., Gorelick, N., & Belward, A. S. (2016). High-resolution mapping of global surface water and its long-term changes. *Nature*, *540*(7633), 418–422. https://doi.org/10.1038/nature20584

Phan, V. H., Lindenbergh, R., & Menenti, M. (2012). ICESat derived elevation changes of Tibetan lakes between 2003 and 2009. *International Journal of Applied Earth Observation and Geoinformation*, *17*, 12–22. https://doi.org/10.1016/j.jag.2011.09.015

Postel, S., & Carpenter, S. (1997). Freshwater ecosystem services. In G. Daily, (Ed.) *Nature's services: Societal dependence on natural ecosystems* (pp. 195–215). Island Press.

Rodell, M., Famiglietti, J. S., Wiese, D. N., Reager, J. T., Beaudoing, H. K., Landerer, F. W., & Lo, M.-H. (2018). Emerging trends in global freshwater availability. *Nature*, *557*(7707), 651–659. https://doi.org/10.1038/s41586-018-0123-1

Schallenberg, M., de Winton, M. D., Verburg, P., Kelly, D. J., Hamill, K. D., Hamilton, D. P., et al. (2013). Ecosystem services of lakes. *Ecosystem Services in New Zealand: Conditions and Trends. Manaaki Whenua Press, Lincoln*, 203–225.

Schwatke, C., Scherer, D., & Dettmering, D. (2019). Automated extraction of consistent time-variable water surfaces of lakes and reservoirs based on Landsat and Sentinel-2. *Remote Sensing*, *11*(9), 1010. https://doi.org/10.3390/rs11091010

Sheng, Y., Song, C., Wang, J., Lyons, E. A., Knox, B. R., Cox, J. S., & Gao, F. (2016). Representative lake water extent mapping at continental scales using multi-temporal Landsat-8 imagery. *Remote Sensing of Environment*, *185*, 129–141. https://doi.org/10.1016/j.rse.2015.12.041

Sterner, R. W., Keeler, B., Polasky, S., Poudel, R., Rhude, K., & Rogers, M. (2020). Ecosystem services of Earth's largest freshwater lakes. *Ecosystem Services*, *41*, 101046. https://doi.org/10.1016/j.ecoser.2019.101046

Tranvik, L. J., Downing, J. A., Cotner, J. B., Loiselle, S. A., Striegl, R. G., Ballatore, T. J., et al. (2009). Lakes and reservoirs as regulators of carbon cycling and climate. *Limnology & Oceanography*, *54*(6part2), 2298–2314. https://doi.org/10.4319/lo.2009.54.6_part_2.2298

Wang, J., Walter, B. A., Yao, F., Song, C., Ding, M., Maroof, A. S., et al. (2022). GeoDAR: Georeferenced global dams and reservoirs dataset for bridging attributes and geolocations. *Earth System Science Data*, *14*(4), 1869–1899. https://doi.org/10.5194/essd-14-1869-2022

Wang, X., Gong, P., Zhao, Y., Xu, Y., Cheng, X., Niu, Z., et al. (2013). Water-level changes in China's large lakes determined from ICESat/GLAS data. *Remote Sensing of Environment*, *132*, 131–144. https://doi.org/10.1016/j.rse.2013.01.005

Williamson, C. E., Saros, J. E., Vincent, W. F., & Smol, J. P. (2009). Lakes and reservoirs as sentinels, integrators, and regulators of climate change. *Limnology & Oceanography*, *54*(6part2), 2273–2282. https://doi.org/10.4319/lo.2009.54.6_part_2.2273

Wohlfahrt, G., Tomelleri, E., & Hammerle, A. (2021). The albedo–climate penalty of hydropower reservoirs. *Nature Energy*, *6*(4), 372–377. https://doi.org/10.1038/s41560-021-00784-y

Woolway, R. I., Kraemer, B. M., Lenters, J. D., Merchant, C. J., O'Reilly, C. M., & Sharma, S. (2020). Global lake responses to climate change. *Nature Reviews Earth & Environment*, *1*(8), 388–403. https://doi.org/10.1038/s43017-020-0067-5

Yang, Q., Shen, X., Anagnostou, E. N., Mo, C., Eggleston, J. R., & Kettner, A. J. (2021). A high-resolution flood inundation archive (2016–the present) from Sentinel-1 SAR imagery over CONUS. *Bulletin of the American Meteorological Society*, *102*(5), E1064–E1079. https://doi.org/10.1175/BAMS-D-19-0319.1

Yao, F., Wang, J., Wang, C., & Crétaux, J.-F. (2019). Constructing long-term high-frequency time series of global lake and reservoir areas using Landsat imagery. *Remote Sensing of Environment*, *232*, 111210. https://doi.org/10.1016/j.rse.2019.111210

Zarfl, C., Lumsdon, A. E., Berlekamp, J., Tydecks, L., & Tockner, K. (2015). A global boom in hydropower dam construction. *Aquatic Sciences*, *77*(1), 161–170. https://doi.org/10.1007/s00027-014-0377-0

Zhang, S., Gao, H., & Naz, B. S. (2014). Monitoring reservoir storage in South Asia from multisatellite remote sensing. *Water Resources Research*, *50*(11), 8927–8943. https://doi.org/10.1002/2014WR015829

Zhao, G., & Gao, H. (2018). Automatic correction of contaminated images for assessment of reservoir surface area dynamics. *Geophysical Research Letters*, *45*(12), 6092–6099. https://doi.org/10.1029/2018GL078343

References From the Supporting Information

McFeeters, S. K. (1996). The use of the Normalized Difference Water Index (NDWI) in the delineation of open water features. *International Journal of Remote Sensing*, *17*(7), 1425–1432. https://doi.org/10.1080/01431169608948714